Inorganic Chemistry

Article

pubs.acs.org/IC

# Structural, Spectroscopic, and Magnetic Properties of $Eu^{3+}$-Doped $GdVO_4$ Nanocrystals Synthesized by a Hydrothermal Method

Agata Szczeszak,[†,‡] Tomasz Grzyb,[†] Zbigniew Śniadecki,[‡,§] Nina Andrzejewska,[†] Stefan Lis,*[,†] Michał Matczak,[‡,∥] Grzegorz Nowaczyk,[∥] Stefan Jurga,[∥,⊥] and Bogdan Idzikowski[‡]

[†]Department of Rare Earths, Faculty of Chemistry, Adam Mickiewicz University, Grunwaldzka 6, 60-780 Poznań, Poland

[‡]Institute of Molecular Physics, Polish Academy of Sciences, M. Smoluchowskiego 17, 60-179 Poznań, Poland

[§]Institute of Nanotechnology, Karlsruhe Institute of Technology (KIT), 76344 Eggenstein-Leopoldshafen, Germany

[∥]Nanobiomedical Centre at Adam Mickiewicz University, Umultowska 85, 61-614 Poznań, Poland

[⊥]Department of Macromolecular Physics, Adam Mickiewicz University, Umultowska 85, 61-614 Poznań, Poland

Supporting Information

**ABSTRACT:** New interesting aspects of the spectroscopic properties, magnetism, and method of synthesis of gadolinium orthovanadates doped with $Eu^{3+}$ ions are discussed. $Gd_{1-x}Eu_xVO_4$ ($x$ = 0, 0.05, 0.2) bifunctional luminescent materials with complex magnetic properties were synthesized by a microwave-assisted hydrothermal method. Products were formed in situ without previous precipitation. The crystal structures and morphologies of the obtained nanomaterials were analyzed by X-ray diffraction and transmission and scanning electron microscopy. Crystallographic data were analyzed using Rietveld refinement. The products obtained were nanocrystalline with average grain sizes of 70−80 nm. The qualitative and quantitative elemental composition as well as mapping of the nanocrystals was proved using energy-dispersive X-ray spectroscopy. The spectroscopic properties of red-emitting nanophosphors were characterized by their excitation and emission spectra and luminescence decays. Magnetic measurements were performed by means of vibrating sample magnetometry. $GdVO_4$ and $Gd_{0.8}Eu_{0.2}VO_4$ exhibited paramagnetic behavior with a weak influence of antiferromagnetic couplings between rare-earth ions. In the substituted sample, an additional magnetic contribution connected with the population of low-lying excited states of europium was observed.

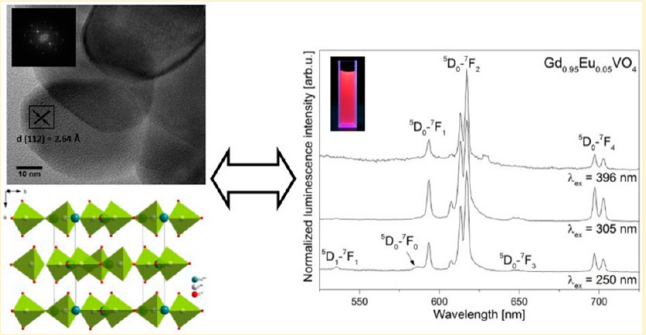


## INTRODUCTION

In the field of inorganic nanophosphors, rare-earth orthovanadates ($REVO_4$) doped with luminescent lanthanide ions ($Ln^{3+}$) play an important role as promising light-emitting materials. Gadolinium orthovanadate ($GdVO_4$) as a host matrix for $Ln^{3+}$ was used for the first time in 1992 by Zaguniennyi et al.,[1] who studied the doped gadolinium orthovanadates as suitable compounds for laser materials. They proved more advantages for this material, such as higher thermal conductivity and broader emission and absorption cross sections, than for yttrium orthovanadate ($YVO_4$). Moreover, matrices based on $Gd^{3+}$ ($4f^7$, $^8S$) have attracted considerable attention as phosphors because of the relatively high energy of the lowest excited state in connection with the stability of the half-filled shell of the ground state of gadolinium.[2] $GdVO_4$ exhibits strong absorption of UV radiation, and such a matrix doped with $Eu^{3+}$ ions is well-known for its efficient and intense red emission, induced by energy transfer from the $VO_4^{3-}$ groups to $Eu^{3+}$ ions.[3] These properties together with good chemical and thermal stability make the $REVO_4$ phosphors good candidates for the production of many optical devices, laser materials, drug delivery systems, magnetic resonance imaging agents, and fluorescent probes.[4−9]

Generally, $REVO_4$ can crystallize in two different phase structures. The first one, possible for all $REVO_4$, is the zircon ($ZrSiO_4$)-type tetragonal crystal system with space group $I4_1/amd$.[10] In this structure, the $Ln^{3+}$ ions occupy one coordination environment with $D_{2d}$ symmetry.[11] The second one is the monazite ($CePO_4$)-type monoclinic structure with space group $P2_1/n$.[12] In this structure, the lanthanide ion is located in the sites with $C_1$ symmetry.[13] The type of product structure depends on the radius of the $RE^{3+}$ ion. Thus, the zircon-type is a stable phase for all $REVO_4$, and the monoclinic structure has been reported only for $LaVO_4$ and $CeVO_4$.[10]

Nowadays, the main goal of nanomaterials synthesis is to obtain high-quality products with good crystallinity, low distribution of grain sizes, and desired morphology. All of these factors strongly influence the luminescence properties, and therefore, several chemical methods are employed in order

Received: February 19, 2014
Published: November 10, 2014

   dx.doi.org/10.1021/ic500354t | Inorg. Chem. 2014, 53, 12243−12252

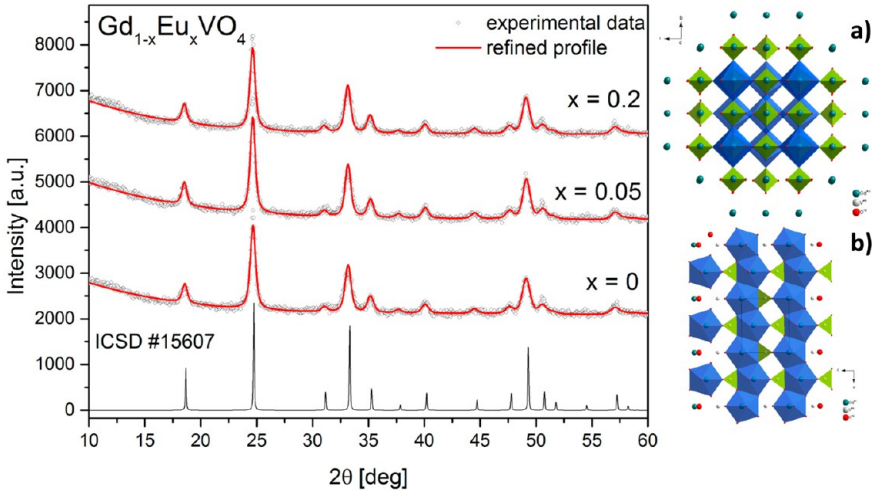


**Figure 1.** (left) Rietveld profile fits of XRD data of $Gd_{1-x}Eu_xVO_4$ ($x$ = 0, 0.05, 0.2) nanocrystals dried at 80 °C for 8 h in air. (right) Crystalline structure of the tetragonal $GdVO_4$ phase: (a) octahedral channels along the $c$ axis and orientation arrangement of $VO_4$ groups; (b) projection of the $GdO_8$ chains along the $c$ and $b$ axes.

to obtain proper nanophosphors. These include electrospinning preparation,[3] the hydrothermal route, surfactant-assisted hydrothermal reactions,[14,15] Pechini's method,[7] and the sol−gel method coupled with hydrothermal conditions.[16] The listed methods give the possibility to produce compounds with wide range of crystallite shapes, such as nanofibers, nanorods, nanotubes, nanobelts, nanospindles, and three-dimensional micro- and nanoparticles.

Recently, the hydrothermal method has been increasingly used in order to prepare nanomaterials with exceptional structural, morphological, and optical properties.[17,18] Moreover, nanophosphors synthesized under hydrothermal conditions can be prepared at relatively low temperature (100−300 °C) without milling or calcination. The hydrothermal route is based on precipitation of products in an aqueous medium under increased pressure and temperature or their recrystallization. Hence, the crystallite size distribution and morphology can be controlled by different factors, e.g., temperature, pH, and the addition of surfactants, which can influence the dissolution or precipitation reaction.[2]

Moreover, besides exceptional luminescence characteristics, rare-earth-based materials exhibit interesting magnetic properties that are strictly connected with the 4f electrons. Fascinating behavior is observed for downscaled systems in which at least one of the dimensions is decreased to nanometers. Multifunctional magnetic nanophosphors are very interesting because of their potential biomedical applications such as magnetic resonance imaging, hyperthermic treatment, and drug delivery.[19,20] However, the magnetic behavior of these materials most often is based on properties of $Fe_3O_4$. Characterization of nanomaterials whose multifunctional properties are connected with $Gd^{3+}$ magnetism and $Ln^{3+}$ emission have still not been fully exploited, especially in the case of $REVO_4$.[21−27]

In the present paper, structural, spectroscopic, and magnetic studies of $Gd_{1-x}Eu_xVO_4$ ($x$ = 0, 0.05, 0.2) are presented and discussed. Here we present new aspects of the luminescence and magnetic properties of the products obtained as well as the method of their synthesis. Detailed analysis of the emission properties, e.g., the asymmetry ratio $R$ and luminescence lifetime, depended on the excitation wavelength used. The magnetic susceptibility was measured in different applied magnetic fields and additionally for the $Eu^{3+}$-doped samples to extend the analysis of the magnetic properties in comparison with previous reports on $REVO_4$ nanocrystals. Moreover, for the first time in this group of nanomaterials, the argumentation is based on a rejection of the giant spin model and the existence of thermally occupied low-lying excited states of $Eu^{3+}$ ions. Additionally, it is very advantageous that a slight modification of the hydrothermal method enabled the nanophosphors to be synthesized without prior precipitation or any additional coreagents and templates, as is usually done.[28] The nanocrystallites were produced in situ by using appropriate solutions of acetate salts of $RE^{3+}$ ions and $NH_4VO_3$ as a vanadium source.

## EXPERIMENTAL SECTION

**Synthesis.** The starting materials $Gd_2O_3$ and $Eu_2O_3$ (Stanford Materials, 99.99%) were dissolved in concentrated acetic acid (Chempur, pure p.a.). The obtained $Gd(CH_3COO)_3$ and $Eu(CH_3COO)_3$ solutions were diluted with distilled water, and 0.25 M solutions were prepared. Then stoichiometric amounts of the appropriate acetate solutions (based on the formula $Gd_{1-x}Eu_xVO_4$ with $x$ = 0, 0.05, 0.2) and a 0.5 M solution of $NH_4VO_3$ (REACHIM, 99%) in 25% excess and heated to 80 °C (added dropwise under vigorous stirring) were mixed. Finally, distilled water was added to the above mixture to reach 70 mL for the total volume, and the pH was adjusted to ∼6.5 using $NH_3$ solution. The as-obtained mixture was transferred to an autoclave and isothermally heated at 180 °C for 3 h. Afterward, it was slowly cooled to room temperature. The synthesized nanocrystals were collected by centrifugation and washed several times with ethanol. The as-prepared yellowish powder was dried at 80 °C for 8 h in air.

**Apparatus.** X-ray diffraction (XRD) patterns were registered using a Bruker AXS D8 Advance diffractometer in the Bragg−Brentano geometry with Cu K$\alpha_1$ radiation ($\lambda$ = 1.541874 Å) in the 2$\theta$ range from 6° to 60°. Transmission electron microscopy (TEM) and high-resolution TEM (HRTEM) images were recorded using an HRTEM JEOL ARM 200F transmission electron microscope at an accelerating voltage of 200 kV. The morphologies of the samples and energy-dispersive X-ray spectroscopy (EDX) analyses were obtained using an FEI NOVA NANOSEM 650 scanning electron microscope. Cell parameters were estimated using Rietveld analysis with the help of the Maud 2.33 software.[29,30]

Luminescence characteristics of the prepared samples were determined using a QuantaMaster 40 spectrophotometer (Photon Technology International) equipped with an Opolette 355LD UVDM tunable laser (Opotek Inc.) as the excitation source and an R928


dx.doi.org/10.1021/ic500354t | Inorg. Chem. 2014, 53, 12243−12252

photomultiplier (Hamamatsu) as a detector. The measurements were done using powder samples at room temperature.

Magnetic data were collected using a Quantum Design Physical Property Measurement System (PPMS) with a vibrating sample magnetometry (VSM) option at temperatures between 2 and 300 K in applied magnetic fields up to 4 T.

## RESULTS AND DISCUSSION

**Structural Analysis.** Figure 1 shows XRD patterns registered for the as-prepared $Gd_{1-x}Eu_xVO_4$ ($x$ = 0, 0.05, 0.2). All of the peaks in the diffraction patterns matched well to the standard diffraction data for bulk $GdVO_4$, corresponding to ICSD card no. 15607. No additional phases of other impurities were observed. Analysis confirmed the formation of a single-phase zircon-type tetragonal product with space group $I4_1/amd$. The well-resolved diffraction peaks indicated the high crystallinity of the materials. These results proved our presumption that highly crystallized nanophosphors can be obtained at a relatively low hydrothermal treatment temperature (180 °C) in a short time of reaction. This is important for such compounds because of the lower possibility of defect formation and thus stronger luminescence.[4] The crystal structure of the $Gd_{1-x}Eu_xVO_4$ nanocrystals was confirmed and the cell parameters were calculated by applying Rietveld analysis. The calculated profiles presented in Figure 1 fit the experimental data well, with residual values not lower than $R_{wp}$ = 3.72. The crystallographic data are summarized in Table 1. The crystal cell parameters are similar to those obtained for the single crystal.[31]

**Table 1. Crystallographic Parameters for Tetragonal $Gd_{1-x}Eu_xVO_4$ ($x$ = 0, 0.05, 0.2) Nanomaterials**

| sample | $a$ (Å) | $c$ (Å) | $V$ (Å$^3$) | $R_{wp}$ (%) |
|---|---|---|---|---|
| $GdVO_4$ | 7.223(0) | 6.373(6) | 332.5(2) | 3.46 |
| $Gd_{0.95}Eu_{0.05}VO_4$ | 7.211(9) | 6.364(1) | 331.0(1) | 3.33 |
| $Gd_{0.8}Eu_{0.2}VO_4$ | 7.216(5) | 6.367(4) | 331.6(1) | 3.72 |

Figure 1a shows schematic presentation of the $GdVO_4$ tetragonal structure. The structure is composed of $VO_4$ tetrahedrons and $GdO_8$ polyhedrons. The $GdO_8$ dodecahedra with $VO_4$ as insets form chains extended along the $c$ axis, while in the $ab$ plane $GdO_8$ dodecahedra are linked by edges. Tetragonal $VO_4$ groups are linked by edge with triangular groups of $GdO_8$ dodecahedra along the $c$ axis, and in the $a$ and $b$ direction $VO_4$ units are connected by corners with $GdO_8$ (Figure 1b).

The size, morphology, and purity of the $GdVO_4$ and $Gd_{0.95}Eu_{0.05}VO_4$ nanoparticles were investigated using TEM, HRTEM, and EDX. In the HRTEM images and fast Fourier transform of the $GdVO_4$ and $Gd_{0.95}Eu_{0.05}VO_4$ nanocrystals (Figures 2a and 3a), the lattice fringes of the crystalline phases can be clearly seen. The interplanar distances between the adjacent lattice fringes are 2.62 Å for the matrix and 2.64 Å for the doped sample, corresponding to $d$(112). As shown in Figures 2b and 3b, the polyhedron-like structures are highly crystalline and slightly agglomerated. The EDX spectra of the orthovanadate nanoparticles confirmed the presence of gadolinium, vanadium, and, in the case of $Gd_{0.95}Eu_{0.05}VO_4$, also europium in the stoichiometric composition without impurities in the samples (Figures 2c and 3c). Moreover, EDX quantitative microanalysis determined a $Eu^{3+}$ ion content of 4.12 ± 0.37% in the $Gd_{0.95}Eu_{0.05}VO_4$ nanophosphor, in good agreement with the intended 5% concentration. The crystallite size distributions calculated on the basis of TEM images are presented in Figures 2d and 3d. They proved that the average grain sizes were 80 ± 10 nm for the undoped material and 70 ± 5 nm for the $Eu^{3+}$-doped sample.

As indicated by the scanning electron microscopy (SEM) images in Figure 4, the samples of $GdVO_4$ and $Gd_{0.95}Eu_{0.05}VO_4$ exhibited the same morphology. The materials consisted of slightly agglomerated cubelike particles. The observed crystallite size of about 70−80 nm was similar to that determined from the TEM analysis.

Additionally, in order to analyze the distribution of Gd, V, and Eu in the nanoparticles, EDX mapping was performed using scanning transmission electron microscopy (STEM), and the results are presented in Figure 5. It was found that the individual elements were distributed uniformly, and there was no clear evidence of significant inhomogeneity in the studied nanocrystals.

**Luminescent Properties.** Figure 6a,c presents the excitation spectra $Gd_{1-x}Eu_xVO_4$ nanocrystals ($x$ = 0.05, 0.2) monitored at $\lambda$ = 620 nm. Both spectra are composed of a broad band in the range 200−350 nm and several weak excitation lines in the range 360−470 nm. The observed broad excitation bands show some irregularities in their shapes. Most probably they are composed of at least four components (excitation bands) that have their maxima at ∼226, ∼250, ∼305, and ∼336 nm. The first maximum can be ascribed to the host absorption band, the second one to $O^{2-}$−$Eu^{3+}$ charge transfer (CT), and the remaining ones to transitions in the $VO_4^{3-}$ group.[32−35] On the basis of the $VO_4^{3-}$ transition bands, the maximum at ∼305 nm is associated with the symmetry-allowed $^1A_1 \rightarrow {}^1T_2$ ($t_1 \rightarrow 2e$) absorption and that at ∼336 nm with the symmetry-forbidden $^1A_1 \rightarrow {}^1T_1$ ($t_1 \rightarrow 2e$) absorption of the $VO_4^{3-}$ unit.[14,36,37] This intense wide peak is an evidence of effectively activated emission of $Eu^{3+}$ ions through energy transfer between $VO_4^{3-}$ groups and $Eu^{3+}$ ions preceded by CT between $V^{5+}$ and $O^{2-}$.[38,39] The energy migration in $Ln^{3+}$-containing systems due to CT was carefully investigated by Faustino et al.[40]

The presented excitation spectra change with increasing concentration of $Eu^{3+}$. The CT band becomes split, and the f−f transition bands much more intense. The cause of the alternations that occur is complex, and at least two effects must be considered to fully understand these observations. It is clearly seen that for the 20% $Eu^{3+}$-doped sample the CT maxima shift toward higher energy. This can be caused by changes in the $O^{2-}$−$Eu^{3+}$ bond elongation and the crystal cell volume.[34] However, the most important reason for the observed changes is a saturation effect, previously described by de Mello Donegá et al.[41] and further confirmed by Trojan-Piegza et al.[42] The obtained vanadates doped with $Eu^{3+}$ absorb light in the region of CT band so effectively that only a part of excitation light can penetrate particles, and the majority of UV photons are absorbed on or near the surface of the nanocrystals. The relatively low absorption coefficients related to the f−f electronic transitions result in much deeper penetration of UV light in the region above 350 nm, and therefore, the f−f transition bands appear to be more intense in higher-doped samples. Another effect is a change in the shape of the wide excitation band connected with $O^{2-}$−$Eu^{3+}$ CT and transitions in the $VO_4^{3-}$ group. Here we also have a fingerprint of the saturation effect and additionally different absorption


dx.doi.org/10.1021/ic500354t | Inorg. Chem. 2014, 53, 12243−12252

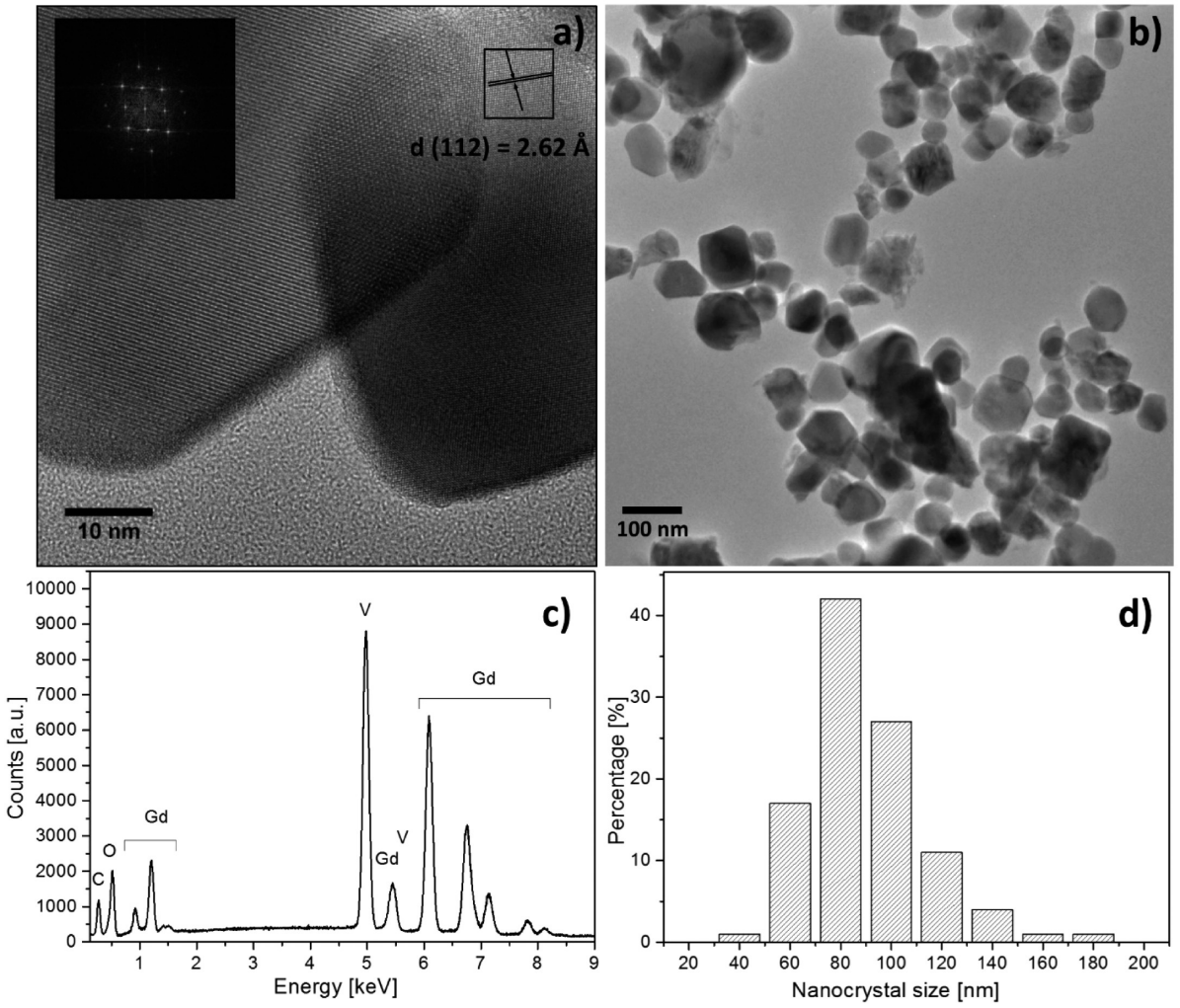


**Figure 2.** (a, b) TEM images, (inset of a) fast Fourier transform image, (c) EDX spectrum, and (d) size distribution of the $GdVO_4$ nanocrystals dried at 80 °C for 8 h in air.

coefficients between the above-mentioned transitions occurring in this region.

A theory that can explain the transfer of energy absorbed by $VO_4^{3-}$ groups to the excited states of $Eu^{3+}$ ions was published in 1948 by Förster[43] and then extended in 1953 by Dexter.[44] This energy transfer (ET) is possible because of overlap of the electric dipole fields of the sensitizer $VO_4^{3-}$groups and the activator $Eu^{3+}$ ions. The absorption cross section of $Ln^{3+}$ ions is several orders of magnitude lower than that of $VO_4^{3-}$ ions as a result of selection rules and forbiddance of f−f transitions.[45] Fortunately, the problem of the low intensity of f−f transitions could be solved by incorporating dopant ions into a suitable matrix. In our case, $Ln^{3+}$ ions occupy crystallographic sites in the $Gd_{1-x}Eu_xVO_4$ structure, and the crystal field diminishes the concentration quenching. The weakly visible lines at >350 nm are connected with the f−f transitions of $Eu^{3+}$ ions. The more intense CT bands confirm that the excitation of the dopant ions is mainly through the $VO_4^{3-}$ units and that efficient ET from the $GdVO_4$ host to the dopant ions occurs.[4,46] Finally, in the nanomaterials based on $Gd_{1-x}Eu_xVO_4$, ET from $Gd^{3+}$ to $Eu^{3+}$ ions is possible. The characteristic sharp band should be visible at about 274 nm, but the CT band overshadows it.

Figure 6b,d presents the emission spectra registered for the different excitation wavelengths. Characteristic of the $Eu^{3+}$ ions, the $^5D_1-^7F_1$ and $^5D_0-^7F_J$ ($J$ = 0−4) transition bands are clearly visible, proving the high crystallinity of the obtained products.[4] The emission intensity of the $^5D_0-^7F_2$ electric dipole transition is hypersensitive and strongly depends on the local site symmetry of the $Eu^{3+}$ ions. The band corresponding to the $^5D_0-^7F_2$ transition is the most intense band in the emission spectrum. However, peaks corresponding to the forbidden $^5D_0-^7F_0$ and $^5D_0-^7F_3$ transitions also appear in the spectrum, showing that $J$-mixing effects are important in this system.[47,48] The $^5D_0-^7F_0$ transition is forbidden by the selection rules, but it is often observed in materials with relatively low symmetries. Among others, it is caused by the above-mentioned $J$-mixing effects, which enable "borrowing" of intensity from the $^5D_0-^7F_J$ ($J$ = 2, 4, 6) transitions, whose probabilities are much higher, as can be explained by Judd−Ofelt theory.[49,50]

As was mentioned earlier, $Eu^{3+}$ ions occupy sites with $D_{2d}$ symmetry without an inversion center. Hence, the $^5D_0-^7F_2$ transition band is relatively more intense compared with the $^5D_0-^7F_1$ magnetic transition band. This is typical when the $Eu^{3+}$ ions are in a low-symmetry environment, as in the investigated sample.

Additionally, the weak lines related to the $^5D_1-^7F_1$ transition band are pronounced. This is possible because of the relatively low vibrational energy of the $VO_4^{3-}$ groups (~880 $cm^{-1}$).[51−53]


dx.doi.org/10.1021/ic500354t | Inorg. Chem. 2014, 53, 12243−12252

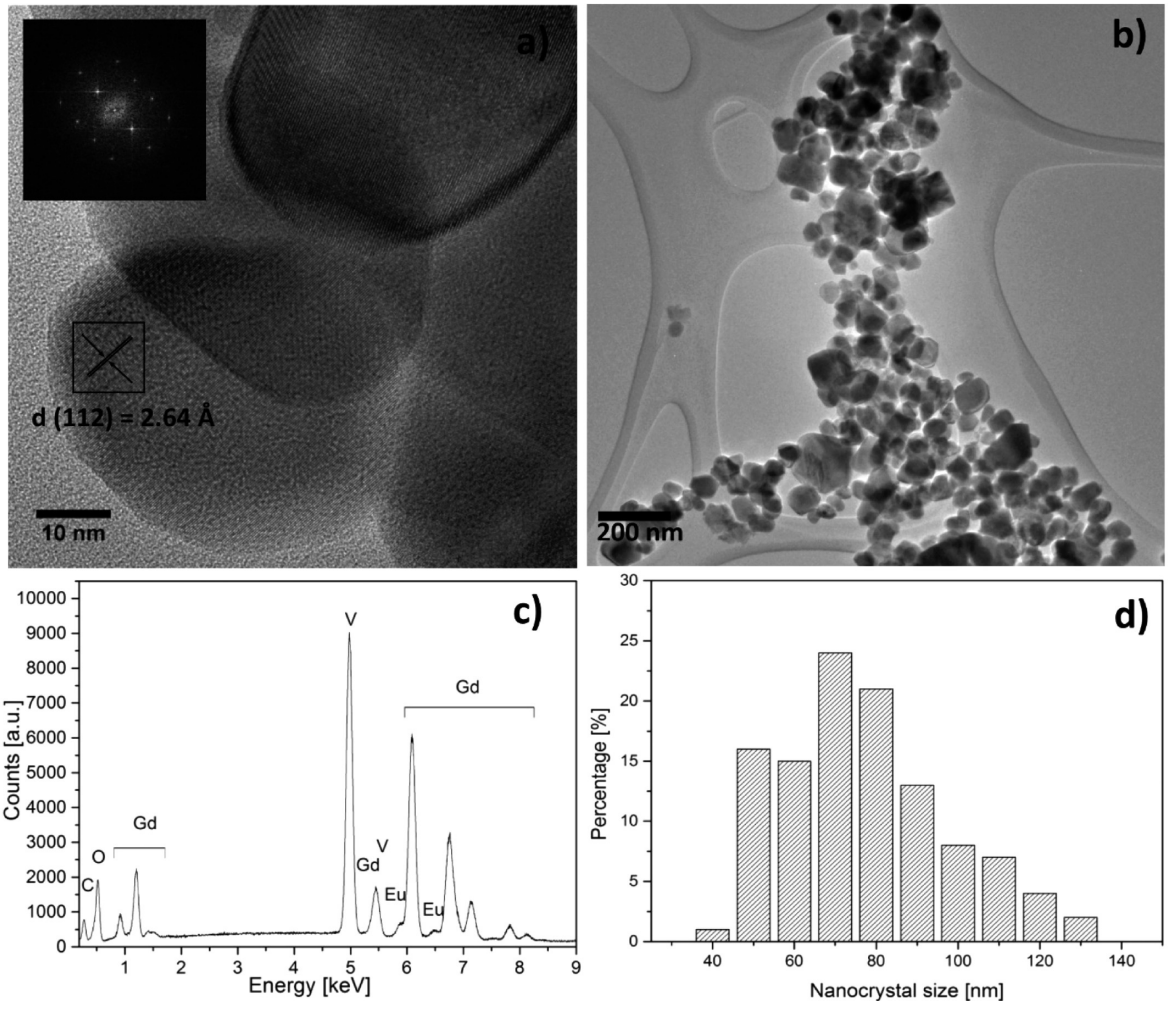


**Figure 3.** (a, b) TEM images, (inset of a) fast Fourier transform image, (c) EDX spectrum, and (d) size distribution of the $Gd_{0.95}Eu_{0.05}VO_4$ nanocrystals dried at 80 °C for 8 h in air.

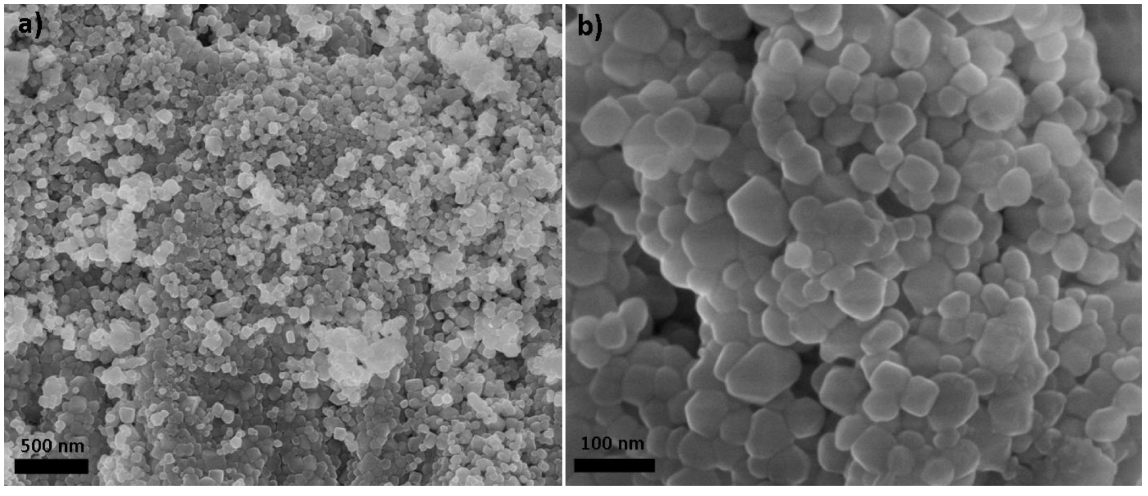


**Figure 4.** SEM images of (a) $GdVO_4$ and (b) $Gd_{0.95}Eu_{0.05}VO_4$ nanocrystals dried at 80 °C for 8 h in air.

Therefore, the probability of multiphonon relaxation between the $^5D_1$ and $^5D_0$ energetic states is low, allowing for emission from the $^5D_1$ state.[54,55]

Generally, a mechanism of the luminescence processes in $Gd_{1-x}Eu_xVO_4$ under UV excitation includes three basic stages. The first step is absorption of UV radiation by the $VO_4^{3-}$ group, and the second step is thermally activated ET to $Eu^{3+}$ ions in the vanadate sublattice. The final step is emission of $Eu^{3+}$ ions excited in this way.[4,5,56]

In order to analyze changes in the site symmetry of the $Eu^{3+}$ ions, the asymmetry parameter *R*, which is the ratio of the integrated intensities of the luminescence bands connected with


dx.doi.org/10.1021/ic500354t | *Inorg. Chem.* 2014, 53, 12243−12252

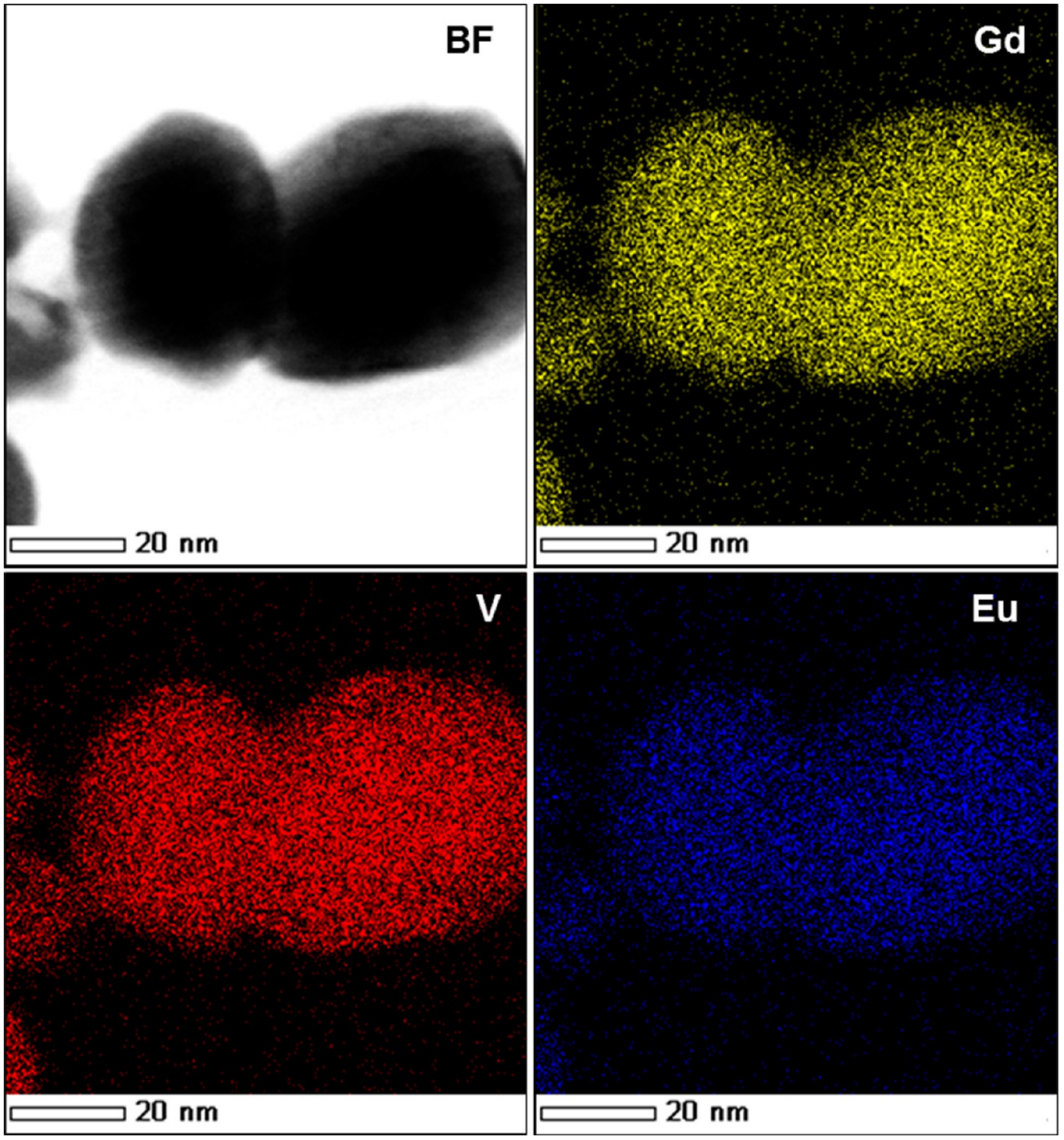


**Figure 5.** Bright-field image of $Gd_{0.95}Eu_{0.05}VO_4$ and EDX maps of Gd, V, and Eu.

the $^5D_0-^7F_2$ and $^5D_0-^7F_1$ transitions, was calculated for each sample.[57] Figure 7 shows the dependence of the asymmetry ratios on the excitation wavelengths for the $Gd_{0.95}Eu_{0.05}VO_4$ and $Gd_{0.8}Eu_{0.2}VO_4$ nanomaterials. The parameter $R$ is different depending on the excitation line because of activation of $Eu^{3+}$ ions occupying sites with distinct symmetry. This means that $Eu^{3+}$ ions can be placed in the $D_{2d}$ site offered by the $GdVO_4$ host and on the crystallite surface. The short time of synthesis can be the reason for the partially amorphous surface of the crystallites and therefore the observed differences (Figure 7 inset). The excitation at $\lambda$ = 396 nm can be interpreted as the one that excites all of the $Eu^{3+}$ ions in the sample, including those with $D_{2d}$ symmetry as well as the ones placed on the surface of the nanocrystallites. On the other hand, the excitation wavelengths $\lambda$ = 250 and 305 nm generate emission characteristic of the lower-symmetry environment of $Eu^{3+}$ ions. The $Gd_{1-x}Eu_xVO_4$ nanocrystals strongly absorb radiation in this region as a result of the absorption of $VO_4^{3-}$ groups. Thus the wavelength of $\lambda$ = 396 nm is more permeable. When $\lambda$ = 396 nm is used as the excitation wavelength, radiation penetrates also the bulk volume of the crystallites, while irradiation at 250 and 305 nm excites mainly the surface dopant ions, which are in the more distorted environment. Particularly, the local symmetry of the $Eu^{3+}$ ions located on the surface of crystallites is disordered because of the amorphous structure. These differences are also reflected in the longer luminescence lifetimes for the $Gd_{0.95}Eu_{0.05}VO_4$ sample, where the participation of less-quenched $Eu^{3+}$ ions is greater at $\lambda$ = 396 nm. In the case of $Gd_{0.8}Eu_{0.2}VO_4$ it is difficult to separate because of the concentration quenching that occurs, which overshadows the other processes.

Figure 8 shows luminescence decay curves for $Gd_{1-x}Eu_xVO_4$ at different concentrations of $Eu^{3+}$ ($x$ = 0.05, 0.2) and excitation wavelengths ($\lambda$ = 250, 305, and 396 nm) monitored at the maximum of the $^5D_0-^7F_2$ transition band. The decay curves had nonexponential character due to the quenching processes,


dx.doi.org/10.1021/ic500354t | Inorg. Chem. 2014, 53, 12243−12252

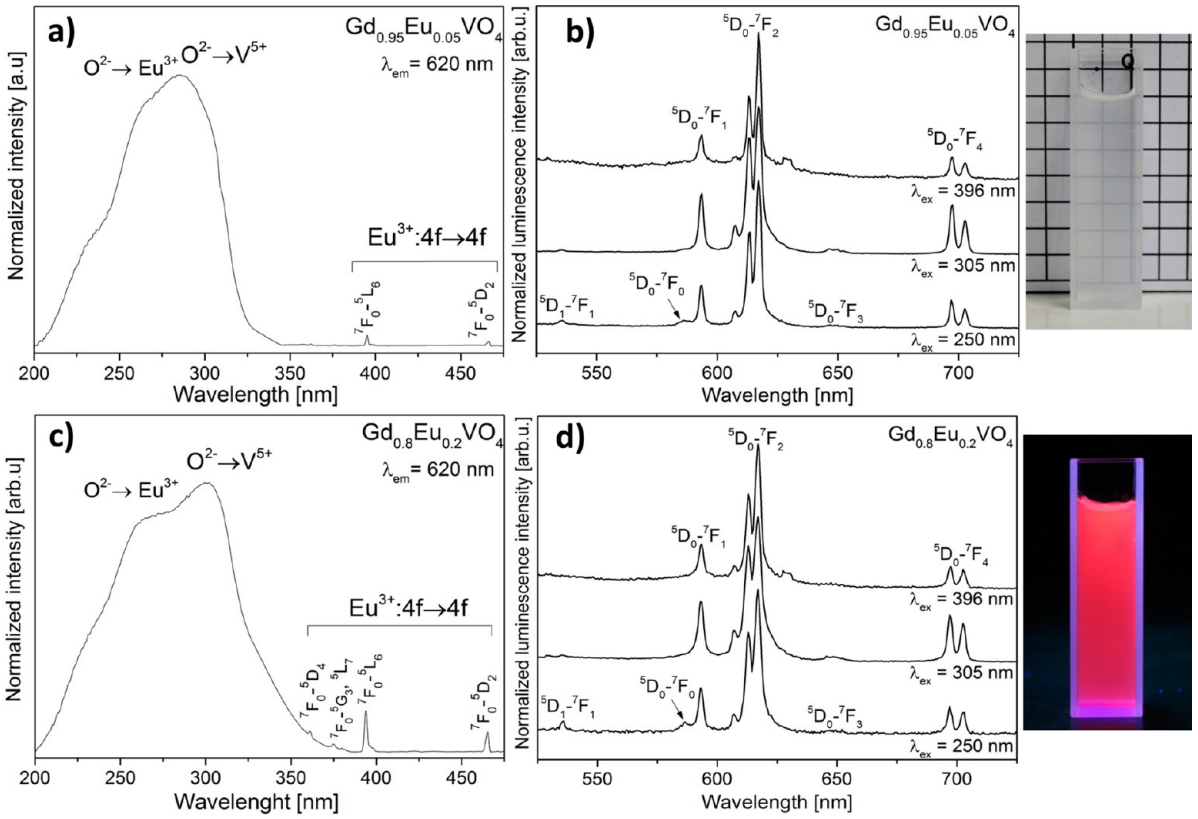


**Figure 6.** (a, c) Excitation and (b, d) emission spectra of $Gd_{1-x}Eu_xVO_4$ nanopowders [(a, b) $x = 0.05$; (c, d) $x = 0.2$] dried at 80 °C for 8 h in air. At the right are shown pictures of the water colloid of $Gd_{0.95}Eu_{0.05}VO_4$ nanopowder in daylight (top) and excited at $\lambda$ = 254 nm (bottom).

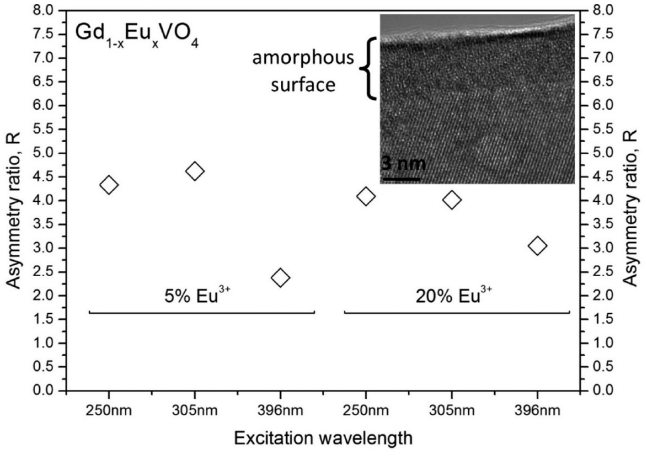


**Figure 7.** Asymmetry parameters $R$ as functions of the excitation wavelengths for the $Gd_{1-x}Eu_xVO_4$ ($x$ = 0.05, 0.2) nanocrystals. The inset is a TEM image showing the amorphous surface of the crystallite.

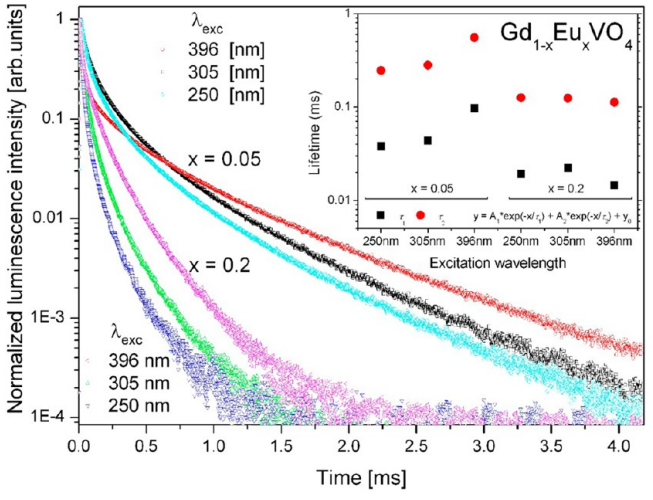


**Figure 8.** Decay curves of $Gd_{1-x}Eu_xVO_4$ dried at 80 °C for 8 h in air. The inset shows calculated values of the luminescence lifetimes for the different $Eu^{3+}$ ion concentrations and excitation wavelengths.

but as an approximation the observed kinetics could be fit using a biexponential function with $R^2$ = 0.998 for $x$ = 0.05 and $R^2$ = 0.993 for $x$ = 0.2. Nonexponential luminescence kinetics can be explained by energy transfer from the excited state of $Eu^{3+}$ ions to impurities, which leads to luminescence quenching.[58,59] Interactions between $Eu^{3+}$ ions in their excited states also lead to nonexponential quenching of luminescence. Two $Eu^{3+}$ ions can transfer energy between them, depopulating the $^5D_0$ excited states and therefore increasing nonradiative energy loss. These effects are especially visible in higher-doped samples. Also, the nanocrystallinity of the prepared samples makes these effects more significant. The shorter components of the luminescence lifetimes can be assigned to activator ions located on the surface of the crystallites, where the environment strongly influences the quenching of the excited states.[17] However, Yang et al.[60] postulated that two components of the luminescence lifetimes could be related to a homogeneous distribution of $Eu^{3+}$ ions inside the orthovanadate matrix without defect centers. Another, which leads to a decrease in the luminescent lifetime, can be associated with $V^{4+}$ defects that cause transfer of the excitation energy to nonradiative recombination routes for electrons and holes. The calculated lifetimes are dependent on


dx.doi.org/10.1021/ic500354t | Inorg. Chem. 2014, 53, 12243−12252

the excitation wavelength used, as is especially visible in case of the 5% $Eu^{3+}$-doped sample. Higher energy of the excitation light (250 and 305 nm) leads to shorter lifetimes as a consequence of quenching the $^5D_0$ excited state of $Eu^{3+}$ ions mostly placed on the amorphous surface, where they are exposed to excitation. Interactions with the $GdVO_4$ host could result in intervalence charge transfer between $Eu^{3+}$ ions and $VO_4^{3-}$ groups.[37] In the case of the higher-doped sample (20%), this effect is less visible because of the dominating role of concentration quenching between $Eu^{3+}$ ions.

**Magnetic Properties.** Magnetic analysis was performed for the matrix and the sample with the highest dopant concentration to observe the effect of Eu substitution most evidently. The temperature dependences of the magnetization $M(T)$ in the zero-field-cooled (ZFC) and field-cooled (FC) regimes were measured over the temperature range from 2 to 300 K (Figure 9, left scale) for $GdVO_4$ and $Gd_{0.8}Eu_{0.2}VO_4$

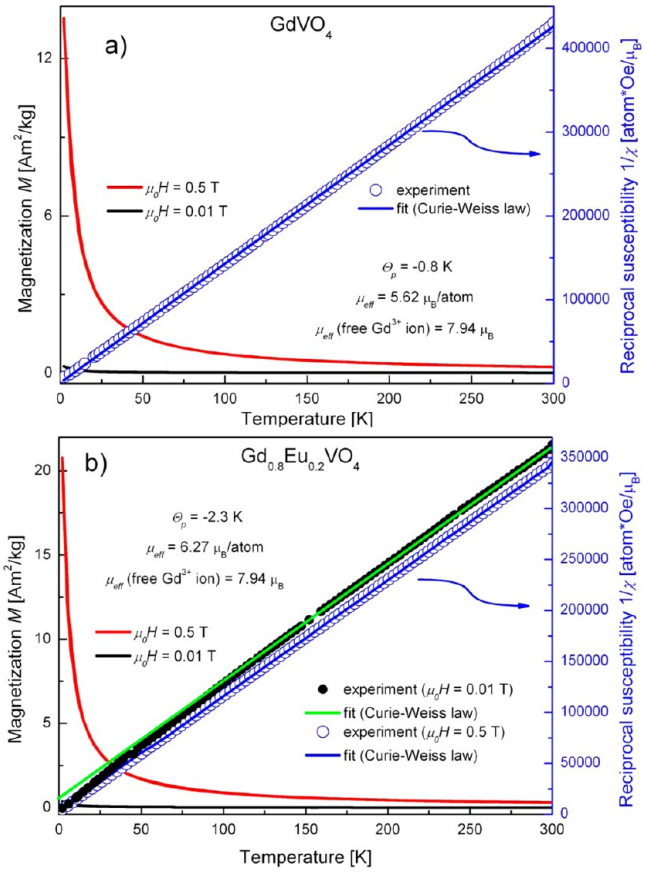


**Figure 9.** Temperature dependence of magnetization $M$ (left scale) and of the reciprocal DC magnetic susceptibility $1/\chi$ (right scale) in (a) $GdVO_4$ and (b) $Gd_{0.8}Eu_{0.2}VO_4$ nanocrystals.

nanocrystals. The two curves coincide over the whole temperature range. The temperature dependence of the reciprocal direct current (DC) magnetic susceptibility was also plotted (Figure 9, right scale) to analyze the magnetic data in detail. The DC magnetic susceptibility was determined at low (0.01 T) and moderate (0.5 T) magnetic fields and is defined as the quotient of $M$ and $H$. The $1/\chi(T)$ dependences measured at 0.5 T show behavior typical for paramagnetic substances. One can observe small deviations, as the paramagnetic Curie temperatures $\Theta_p$ are slightly negative and equal to −1 and −2 K for $GdVO_4$ and $Gd_{0.8}Eu_{0.2}VO_4$, respectively. The effective magnetic moments per magnetic ion ($\mu_{eff}$) are smaller than in free $Gd^{3+}$ and amount to $5.62\mu_B$ for $GdVO_4$ and $6.27\mu_B$ for $Gd_{0.8}Eu_{0.2}VO_4$. Low-field measurements are not so unambiguous, and $1/\chi(T)$ for the Eu-substituted sample deviates from the Curie−Weiss behavior (Figure 9b). The reciprocal susceptibility curve bends downward and approaches the origin of coordinates at low temperatures. The effective magnetic moments calculated from the low-field measurements are similar to those measured for $\mu_0H$ = 0.5 T and are equal to $5.64\mu_B$ for $GdVO_4$ and $6.23\mu_B$ for $Gd_{0.8}Eu_{0.2}VO_4$. The temperature dependence of $1/\chi$ for the substituted sample was fitted with Curie−Weiss formula at high temperatures (above 150 K). The paramagnetic Curie temperature of $\Theta_p$ = −14 K determined from the measurements at moderate magnetic field cannot be taken as an explicit indication of antiferromagnetic interactions between nanoparticles because in this case $1/\chi(T)$ should deviate upward with decreasing temperature. For these nanoparticles,[61] it was concluded that such behavior was connected with a typical paramagnetic system with independent dynamics of the magnetic moment of each rare-earth ion.

The magnetic field dependence of the magnetization in $GdVO_4$ and $Gd_{0.8}Eu_{0.2}VO_4$ nanocrystals was measured at four fixed temperatures. The results for $GdVO_4$ are presented as an example in Figure 10. Saturation of magnetization was not

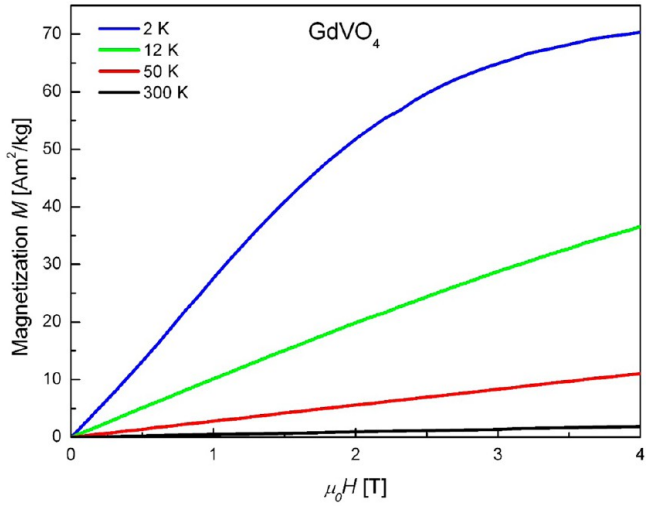


**Figure 10.** Magnetization as a function of magnetic field in $GdVO_4$ nanocrystals.

observed up to $\mu_0H$ = 4 T. The curves for both samples do not exhibit any hysteresis and at high temperatures (above 50 K) point out typical paramagnetic behavior. The low-temperature $M(H)$ dependence could indicate superparamagnetism, but there are indisputable arguments in contradiction with such an interpretation. At first, the FC and ZFC $M(T)$ curves do not deviate from each other, and there is no cusp down to 2 K. This could indicate an ultralow blocking temperature,[61,62] despite the relatively large diameters of nanoparticles and high content of $Gd^{3+}$ ions. Besides that, there is a strong deviation of the $M(H/T)$ curves measured at different temperatures (Figure 11), whereas these curves should superimpose for superparamagnetic behavior.

To summarize, the results obtained from the $M(T)$ and $M(H)$ measurements could indicate that $GdVO_4$ behaves as a paramagnet but with signs of antiferromagnetic coupling in the


dx.doi.org/10.1021/ic500354t | Inorg. Chem. 2014, 53, 12243−12252

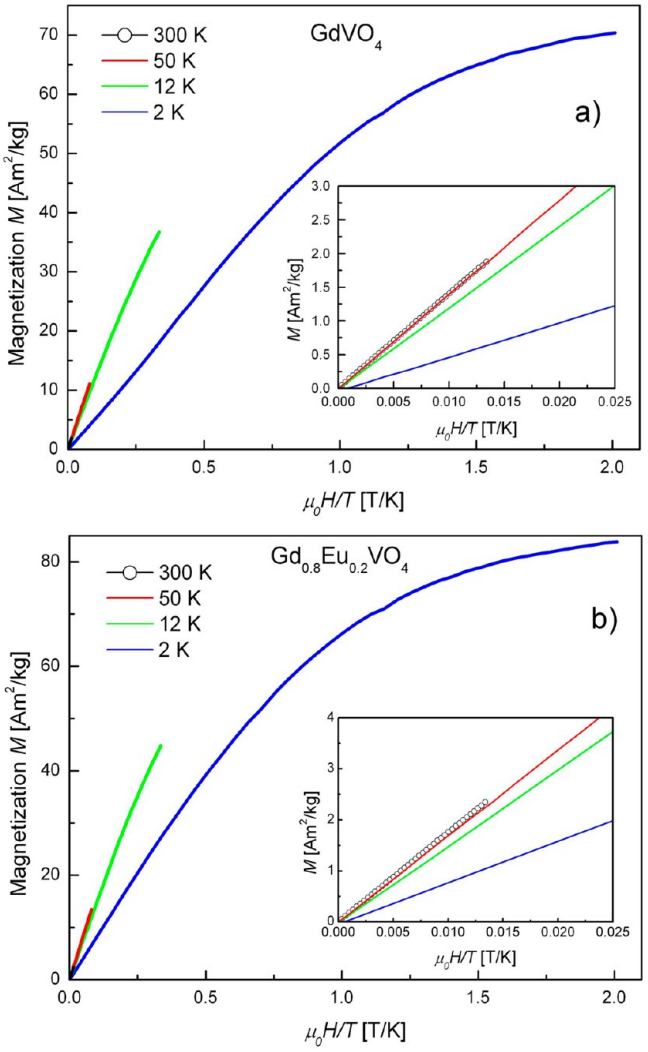


**Figure 11.** Magnetization as a function of magnetic field and temperature in $GdVO_4$ (a) and $Gd_{0.8}Eu_{0.2}VO_4$ (b) nanocrystals.

Gd sublattice. There is slightly negative paramagnetic Curie temperature, and the $M(H/T)$ curves do not superimpose on each other. The deviation is stronger at lower temperatures, approaching the expected ultralow-temperature transition to a magnetically ordered phase. As reported previously for $Er^{3+}$-doped nanoparticles,[61] the magnetic moments on rare-earth ions in such systems can behave independently. An ultralow blocking temperature can be connected with negligible magnetic interactions between rare-earth ions and several orders of magnitude lower magnetic moments of single ions in comparison with giant spins in the case of a typical superparamagnet.[63] The exchange interactions between the lanthanide ions are reduced because the 4f shells are shielded by full outer shells. The deviations of $1/\chi(T)$ for the Eu-substituted sample could be connected with the contributions from low-lying excited states possessing magnetic moments that differ from those of the ground state. This effect was observed only for the Eu-containing sample, where the magnetic $^7F_{1,2,3}$ states are very close to the $^7F_0$ nonmagnetic ground state. Therefore, additional magnetic contribution can be induced by the population of excited states according to Boltzmann statistics at higher temperatures.[64] In accordance with this, one can observe a smaller slope of $1/\chi(T)$ and thus an increase in the effective magnetic moment with increasing temperature (Figure 10b, $1/\chi(T)$ measured at 0.01 T). Application of higher magnetic fields causes larger splitting of energy levels and decreases the probability of depopulation of the nonmagnetic ground state, as can be seen in the temperature dependence of the reciprocal magnetic susceptibility measured at 0.5 T. The described effect overlaps with those observed for $GdVO_4$ and is connected with the existence of antiferromagnetic couplings. Ultralow-temperature measurements would be conclusive and give clear evidence for this complex behavior.

## CONCLUSIONS

Nanocrystalline $Gd_{1-x}Eu_xVO_4$ materials were synthesized under hydrothermal conditions without prior precipitation of the precursor and additional coreagents. Detailed structural and morphological analyses were carried out and indicated the formation of single-phase tetragonal nanocrystals. Intense red emission of the obtained nanophosphors due to doping with the $Eu^{3+}$ ions was observed and arises from transitions occurring between the $^5D_0$ excited state and $^7F_J$ ground states of these ions. The visible emission was activated mainly by charge transfer in the $VO_4^{3-}$ groups and subsequent energy transfer to the dopant ions. The observed spectroscopic properties of the obtained materials were strongly influenced by their complex structure and morphology, showing differences between ions placed on the surface and inside of the nanocrystals.

The magnetic properties of $GdVO_4$ and $Gd_{0.8}Eu_{0.2}VO_4$ nanocrystals are complex, considering the occurrence of paramagnetism with independent behavior of each rare-earth ion and additional effects connected with the weak antiferromagnetic couplings. A deviation from the Curie–Weiss law was observed for the Eu-substituted sample and was assigned to a magnetic contribution from low-lying $^7F_{1,2,3}$ excited states, which are populated with increasing temperature.

The bifunctional luminescence and magnetic characteristics of $Gd_{1-x}Eu_xVO_4$ nanophosphors enable these materials to be used as promising candidates for advanced applications. Because of their unique magnetic properties, such systems are good candidates for numerous applications, such as nanoscale refrigeration at ultralow temperatures.

## ASSOCIATED CONTENT

### Supporting Information

Revised crystallographic data for tetragonal $GdVO_4$ nanocrystals in CIF format. This material is available free of charge via the Internet at http://pubs.acs.org.

## AUTHOR INFORMATION

### Corresponding Author

*Fax: +48 618291505. Tel: +48 618291345. E-mail: blis@amu.edu.pl.

### Notes

The authors declare no competing financial interest.

## ACKNOWLEDGMENTS

Funding for this research was provided by the National Science Centre (Grant DEC-2012/06/M/ST5/00325). T.G. holds a scholarship from the Foundation for Polish Science for Young Scientists (FNP). This work was partially supported through an Iuventus Plus Grant (IP2011 055671 to Z.S.) from the Polish Ministry of Science and Higher Education and by the National

Centre for Research and Development (PBS1/A9/13/2012 to G.N.).

## REFERENCES


(1) Zaguniennyi, A. I.; Ostoumov, V. G.; Shcherbakov, I. A.; Jensen, T.; Meyn, J. P.; Huber, G. *J. Quantum Electron.* **1992**, *22*, 1071−1072.
(2) Wu, J.; Yan, B. *J. Alloys Compd.* **2008**, *455*, 485−488.
(3) Li, X.; Yu, M.; Hou, Z.; Li, G.; Ma, P.; Wang, W.; Cheng, Z.; Lin, J. *J. Solid State Chem.* **2011**, *184*, 141−148.
(4) Xu, Z.; Feng, B.; Gao, Y.; Zhao, Q.; Sun, D.; Gao, X.; Li, K.; Ding, F.; Sun, Y. *CrystEngComm* **2012**, *14*, 5530−5538.
(5) Wang, F.; Xue, X.; Liu, X. *Angew. Chem., Int. Ed.* **2008**, *47*, 906−909.
(6) Zhang, J.; Wang, Y.; Xu, Z.; Zhang, H.; Dong, P.; Guo, L.; Li, F.; Xin, S.; Zeng, W. *J. Mater. Chem. B* **2013**, *1*, 330−338.
(7) Huang, S.; Cheng, Z.; Ma, P.; Kang, X.; Dai, Y.; Lin, J. *Dalton Trans.* **2013**, *42*, 6523−6530.
(8) Shie, N.-C.; Hsieh, W.-F.; Shy, J.-T. *Opt. Express* **2011**, *19*, 21109−21115.
(9) Gai, S.; Yang, P.; Wang, D.; Li, C.; Niu, N.; He, F.; Zhang, M.; Lin, J. *Advances* **2012**, *2*, 3281−3287.
(10) *Handbook on the Physics and Chemistry of Rare Earths*, Vol. *34*; Gschneidner, K. A., Jr., Bünzli, J.-C. G., Pecharsky, V. K., Eds.; Elsevier: Amsterdam, 2004.
(11) Yan, B.; Wu, J.-H. *Mater. Lett.* **2009**, *63*, 946−948.
(12) Cong, H.; Zhang, H.; Sun, S.; Yu, Y.; Yu, W. *J. Appl. Crystallogr.* **2010**, *43*, 308−319.
(13) Kang, J. H.; Im, W. B.; Lee, D. C.; Kim, J. Y.; Jeon, D. Y.; Kang, Y. C.; Jung, K. Y. *Solid State Commun.* **2005**, *133*, 651−656.
(14) Yang, L.; Li, L.; Zhao, M.; Li, G. *Phys. Chem. Chem. Phys.* **2012**, *14*, 9956−9965.
(15) Choi, S.; Moon, Y.-M.; Jung, H.-K. *J. Lumin.* **2010**, *130*, 549−553.
(16) Calderón-Villajos, R.; Zaldo, C.; Cascales, C. *CrystEngComm* **2012**, *14*, 2756−2768.
(17) Szczeszak, A.; Grzyb, T.; Barszcz, B.; Nagirnyi, V.; Kotlov, A.; Lis, S. *Inorg. Chem.* **2013**, *52*, 4934−4940.
(18) Grzyb, T.; Runowski, M.; Szczeszak, A.; Lis, S. *J. Solid State Chem.* **2013**, *200*, 76−83.
(19) Berry, C. C. *J. Phys. D: Appl. Phys.* **2009**, *42*, 22403−22012.
(20) Andrä, W.; Häfeli, U.; Hergt, R.; Misri, R. In *Handbook of Magnetism and Advanced Magnetic Materials, Vol. 4: Novel Materials*; Kronmüller, H., Parkin, S., Eds.; Wiley: Chichester, U.K., 2007.
(21) Wong, H.-T.; Chan, H. L. W.; Hao, J. H. *Appl. Phys. Lett.* **2009**, *95*, No. 022512.
(22) Das, G. K.; Heng, B. C.; Ng, S.-C.; White, T.; Loo, J. S. C.; D'Silva, L.; Padmanabhan, P.; Bhakoo, K. K.; Selvan, S. T.; Tan, T. T. Y. *Langmuir* **2010**, *26*, 8959−8965.
(23) Johnson, N. J. J.; Oakden, W.; Stanisz, G. J.; Prosser, R. S.; Van Veggel, F. C. J. M. *Chem. Mater.* **2011**, *23*, 3714−3722.
(24) Ren, G.; Zeng, S.; Hao, J. *J. Phys. Chem. C* **2011**, *115*, 20141−20174.
(25) Setua, S.; Menon, D.; Asok, A.; Nair, S.; Koyakutty, M. *Biomaterials* **2010**, *31*, 714−729.
(26) Zeng, S.; Xiao, J.; Yang, Q.; Hao, J. *J. Mater. Chem.* **2012**, *22*, 9870−9874.
(27) Zhou, J.-C.; Sun, L.-D.; Shen, J.; Gu, J.-Q.; Yan, C.-H. *Nanoscale* **2011**, *3*, 1977−1983.
(28) Liu, G.; Duan, X.; Li, H.; Dong, H.; Zhu, L. *J. Cryst. Growth* **2008**, *310*, 4689−4696.
(29) Rietveld, H. M. *J. Appl. Crystallogr.* **1969**, *2*, 65−71.
(30) Lutterotti, L.; Bortolotti, M. *Compcomm. Newsl.* **2003**, *1*, 43−50.
(31) Kochurikhin, V. V.; Shimamura, K.; Fukuda, T. *J. Cryst. Growth* **1995**, *151*, 393−395.
(32) Wang, J.; Xu, Y.; Hojamberdiev, M.; Cui, Y.; Liu, H.; Zhu, G. *J. Alloys Compd.* **2009**, *479*, 772−776.
(33) Liu, D.; Shi, J.; Tong, L.; Ren, X.; Li, Q.; Yang, H. *J. Nanopart. Res.* **2012**, *14*, 1216−1223.
(34) Yang, H. K.; Moon, B. K.; Choi, B. C.; Jeong, J. H.; Kim, K. H. *CrystEngComm* **2011**, *13*, 4723−4728.
(35) Liu, G.; Hong, G.; Wang, J.; Dong, X. *Nanotechnology* **2006**, *17*, 3134−3138.
(36) Ronde, H.; Blasse, G. *J. Inorg. Nucl. Chem.* **1978**, *40*, 215−219.
(37) Krumpel, A. H.; van der Kolk, E.; Cavalli, E.; Boutinaud, P.; Bettinelli, M.; Dorenbos, P. *J. Phys.: Condens. Matter* **2009**, *21*, No. 115503.
(38) Singh, S.; Tripathi, A.; Kumar Rastogi, C.; Sivakumar, S. *Advances* **2012**, *2*, 12231−12236.
(39) Stouwdam, J. W.; Raudsepp, M.; Van Veggel, F. C. J. M. *Langmuir* **2005**, *21*, 7003−7008.
(40) Faustino, W. M.; Malta, O. L.; de Sá, G. F. *J. Chem. Phys.* **2005**, *122*, 54109−54119.
(41) De Mello Donegá, C.; Meijerink, A.; Blasse, G. *J. Lumin.* **1994**, *62*, 189−201.
(42) Trojan-Piegza, J.; Zych, E.; Hreniak, D.; Strek, W.; Kepinski, L. *J. Phys.: Condens. Matter* **2004**, *16*, 6983−6994.
(43) Forster, Th. *Ann. Phys.* **1948**, *2*, 55−75.
(44) Dexter, D. L. *J. Chem. Phys.* **1953**, *21*, 836−850.
(45) Weber, M. J. *Phys. Rev. B* **1973**, *8*, 54−64.
(46) Shanta Singh, N.; Ningthoujam, R. S.; Phaomei, G.; Singh, S. D.; Vinu, A.; Vatsa, R. K. *Dalton Trans.* **2012**, *41*, 4404−4412.
(47) Tanaka, M.; Nishimura, G.; Kushida, T. *Phys. Rev. B* **1994**, *49*, 16917−16925.
(48) Tanaka, M.; Kushida, T. *J. Alloys Compd.* **1993**, *193*, 183−185.
(49) Judd, B. *Phys. Rev.* **1962**, *127*, 750−761.
(50) Ofelt, G. S. *J. Chem. Phys.* **1962**, *37*, 511−520.
(51) Miller, S. A.; Caspers, H. H.; Rast, H. E. *Phys. Rev.* **1968**, *168*, 964−969.
(52) Kaminskii, A. A.; Ueda, K.; Eichler, H. J.; Kuwano, Y.; Kouta, H.; Bagayev, S. N.; Chyba, T. H.; Barnes, J. C.; Murai, T.; Lu, J. *New Opt. Mater.* **2001**, *11*, 1124−1133.
(53) Pan, G.; Song, H.; Bai, X.; Liu, Z.; Yu, H.; Di, W.; Li, S.; Fan, L.; Ren, X.; Lu, S. *Chem. Mater.* **2006**, *18*, 4526−4532.
(54) Wang, D.; Yang, P.; Cheng, Z.; Wang, W.; Ma, P.; Zhai, X.; Lin, J. *J. Nanopart. Res.* **2012**, *14*, 707−717.
(55) Yu, M.; Lin, J.; Wang, Z.; Fu, J.; Wang, S.; Zhang, H. J.; Han, Y. C. *Chem. Mater.* **2002**, *14*, 2224−2231.
(56) Blasse, G. *J. Chem. Phys.* **1966**, *45*, 2356−2360.
(57) Liao, Y.; Zhan, Y.; Chen, N.; Du, G. *J. Sol-Gel Sci. Technol.* **2012**, *65*, 353−358.
(58) Huber, D. *Phys. Rev. B* **1979**, *20*, 2307−2314.
(59) Riwotzki, K.; Meyssamy, H.; Kornowski, A.; Haase, M. *J. Phys. Chem. B* **2000**, *104*, 2824−2828.
(60) Yang, L.; Li, G.; Zhao, M.; Zheng, J.; Guan, X.; Li, L. *Nanotechnology* **2012**, *23*, No. 245602.
(61) Van den Heuvel, W.; Tikhomirov, V. K.; Kirilenko, D.; Schildermans, N.; Chibotaru, L. F.; Vanacken, J.; Gredin, P.; Mortier, M.; van Tendeloo, G.; Moshchalkov, V. V. *Phys. Rev. B* **2010**, *82*, No. 094421.
(62) Grzyb, T.; Gruszeczka, A.; Wiglusz, R. J.; Śniadecki, Z.; Idzikowski, B.; Lis, S. *J. Mater. Chem.* **2012**, *22*, 22989−22997.
(63) Bedanta, S.; Kleemann, W. *J. Phys. D: Appl. Phys.* **2009**, *42*, 13001−13028.
(64) Kachkanov, V.; Wallace, M. J.; van der Laan, G.; Dhesi, S. S.; Cavill, S. a; Fujiwara, Y.; O'Donnell, K. P. *Sci. Rep.* **2012**, *2*, 969−974.